JOURNAL OF MATERIALS SCIENCE 26 (1991) 6458–6466

Two-melt separation in supercooled Cu–Co alloys solidifying in a drop-tube

A. MUNITZ*, R. ABBASCHIAN
Department of Materials Science and Engineering, University of Florida, Gainesville, FL 32611, USA

The microstructure of Cu–Co alloys solidified by a free-fall containerless solidification was investigated using scanning electron microscopy. Spherical Cu–Co drops of about 3 mm diameter were solidified in an evacuated 105 m long drop-tube. The microstructures were compared with those obtained by an electromagnetic levitation technique. It was found that the falling drops were at the "liquid + solid" state at the moment of impact on the floor. Upon bumping on to the floor the drop splits into many fragments, which finally solidify in the form of flakes upon retouching the tube floor. The microstructure depends mainly on the solid fraction in the flake, and on its temperature at the moment of impact. Supercoolings up to $0.2T_M$ could be achieved within the drop-tube, causing separation of the liquid into two melts. Under certain conditions the microstructure reveals the occurrence of discarded spheres, suggesting that cooling below a certain temperature (T_{misc}) will cause mixing of the two melts into one liquid. Interpretation of the observed microstructures is based on the current understanding of rapid solidification mechanisms.

1. Introduction

In the past several years there has been an increased interest in utilizing an orbital space environment to carry out low-gravity solidification experiments. These experiments offer unique advantages, such as containerless growth of single crystals of very low impurity content. Such processing eliminates reaction with the container, leading to reduction in contamination, as well as eliminating heterogeneous nucleation at the container wall. Large-bulk supercooling could then occur, which in turn leads to a diversity of solidification modes; for example, partitionless (massive) solidification where the solid has the same solute concentration as the parent liquid [1–3]. In addition, the supercooling may change the solidification morphology from dendritic to non-dendritic [4–6], may allow the formation of alternate phases [7], and/or refine the grain size [8, 9]. Another important effect of bulk melt supercooling, which has not yet been studied extensively, is its effect on the microstructure of alloys which exhibit a metastable miscibility gap, such as the Cu–Co and Cu–Fe systems. The supercooling of these alloys has recently been investigated by the use of electromagnetic (EM) levitation [10, 11]. It was found that the supercooling of the melt below a certain limit causes separation into two melts, each of which solidifies in a different path dictated by the metastable phase boundaries. However, EM levitation induces strong fluid flow during solidification, which enhances coarsening and dendrite arm breakage, altering the inherent solidification behaviour.

A containerless low-gravity environment can be simulated on earth for short periods of time (1–6 s) by using the long drop-tube technique. In 1956 Cech and Turnbull [12] used a short drop-tube to obtain supercooling in small molten droplets. More recently, Meyer and Rinderer [13] and Nelson [14] reported the supercooling of small molten drops of refractory metals in the range of about $0.29T_M$ (where T_M is the absolute melting temperature). Such high supercooling is claimed to be possible due to the lack of convection, which avoids dynamic nucleation.

In this work, the solidification of Cu–Co alloys in the 105 m drop-tube at the NASA Marshal Space-Flight Center (NSFC) was investigated. The microstructure obtained was compared with those revealed in specimens solidified from various levels of bulk supercooling in an EM levitation apparatus. There are three main differences between solidification conditions in a drop-tube and EM levitation: (i) in the drop-tube only radiative cooling exists, while in EM levitation conductive cooling also exists due to the flow of He; (ii) no convection exists in the drop-tube during solidification, while in EM levitation there is large convection due to the magnetic forces; and (iii) there is a large momentum transfer at the impact moment in the drop-tube due to the 105 m free fall, while using EM levitation there is almost no momentum transfer.

The Cu–Co phase diagram has been thermodynamically modelled for both stable and metastable equilibria [15–18]. The calculated diagrams show a

* Visiting Research Associate from Nuclear Research Center, Nagev, PO Box 9001, Beer-Sheva, Israel.

0022–2461/91 $03.00 + .12

metastable miscibility gap in the solid-plus-liquid region. There is, however, little experimental support for the existence of the metastable miscibility gap [10, 19]. The major goal of the present work was to study the effects of supercooling on the microstructure of Cu–Co alloys using the drop-tube, and to compare the results with those obtained by EM levitation [10].

2. Experimental procedure

Samples of the desired composition were prepared by arc-melting of high-purity cobalt (99.99%) and copper (99.98%) in an atmosphere of Ar with 2 wt % H_2. The arc-melted specimens, weighing approximately 0.5 g, were placed in a levitation melting apparatus located in a bell-jar on top of the 105 m drop-tube. The tube was evacuated to about 10^{-5} torr by turbomolecular vacuum pumps. The specimen was suspended and heated by an r.f. heating coil. Its temperature was measured by a two-colour pyrometer. A typical thermal history of a Cu–Co alloy is summarized in Fig. 1. When the desired temperature was obtained, the power to the levitator was shut down, allowing the specimen to free-fall for 4.61 s. During the fall, three Si infrared detectors, located at the 15th, 9th and 7th floors (the one on the 7th floor looks upward while the others look downward) measure the changes in the sample brightness as a function of fall time (Fig. 2). Fig. 2a shows a typical thermal history output (temperature as a function of fall time) of a sample solidified without supercooling, while Fig. 2b and c show a sample solidified with deep bulk supercooling. The sharp increase in brightness at around 4.4 s (this region is shown with higher amplification in Fig. 2c) is due to the rapid latent heat release during recalescence. The recalescence temperature may be determined from the heat loss calculated during the time the sample is dropped until the recalescence time (see Section 4 below). It turns out that after solidification the sample attained the form of fine powder, as seen in Fig. 3. This shows a macro-photograph of the powder that was collected from the drop-tube floor as well as a specimen which solidified during the levitation.

Another set of samples was processed by EM levitation. The details of sample processing via EM levitation is described elsewhere [1].

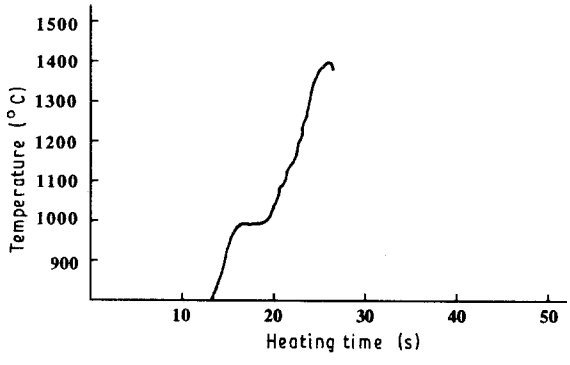

Figure 1 Typical thermal history measured by the pyrometer, illustrating the dropping temperature.

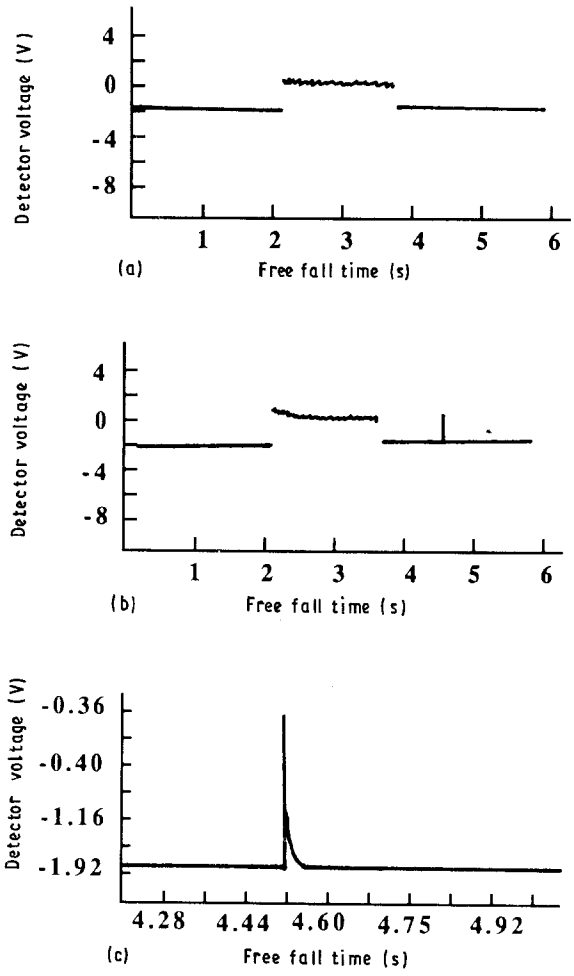

Figure 2 Typical output of the top Si detector, illustrating (a) a sample which solidified without supercooling and (b) a sample solidified with about 300 K supercooling. (c) The peak signal at 4.4 s caused by rapid heat of fusion release during the recalescence, at high resolution.

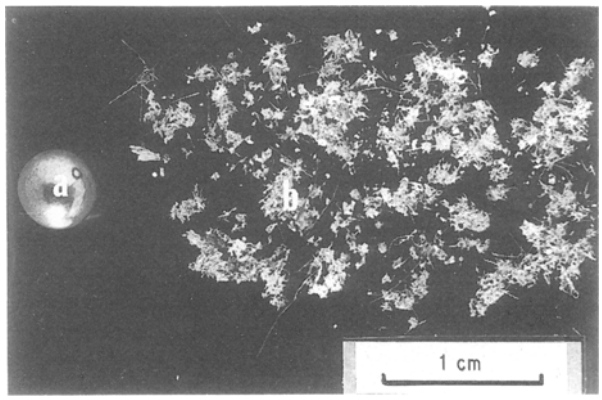

Figure 3 Overall view showing the original Cu–Co sphere (a) and the flakes received on the drop-tube bottom (b).

After solidification, the powder particles were suspended in transparent epoxy. They were then carefully polished, starting with a 600 grit SiC abrasive paper. Then the samples were polished on a soft cloth with diamond paste down to a 0.25 μm grit. Final polish was obtained with 0.05 μm grit alumina. The specimens were then etched in a solution of 120 ml H_2O and 10 g of ammonium cupric chloride, adding ammonium hydroxide until all the crystals of ammonium

cupric chloride dissolved. The etching time ranged between 5 and 12 s. Microstructural as well as X-ray microanalysis were carried out using a scanning electron microscope (SEM, Philips type 505 with energy-dispersive spectroscopy (EDS) capabilities). For the X-ray microanalysis, the specimens were etched very lightly in order to reveal the microstructure, while keeping errors arising from geometrical effects to a minimum. The raw data were corrected with a standard ZAF computer program [20] (Z = atomic number, A = absorption, F = fluorescence, including background as well as dead-time corrections). This technique was capable of making reliable compositional analysis of particles larger than 5 μm.

3. Results

A series of secondary electron images illustrating the characteristic microstructure of Cu–15 wt % Co solidified via EM levitation and drop-tube experiments are shown in Figs 4 and 5, respectively. Fig. 4a shows the microstructure of specimens which were cooled to a temperature in the "liquid + solid" region of the phase diagram [19] during levitation, and quenched on a copper plate starting from that temperature. The solidification starting from this temperature occurs in a "normal" manner, with nucleation of the primary α-Co dendrite (bright particles in the figures), containing approximately 82–83 wt % Co. Solidification proceeds by a peritectic reaction, which results in an ε-Cu phase growing around the primary α-Co dendrites until the dendrites are completely surrounded. At this point the ε-Cu solidifies directly from the melt in a dendritic mode. The centre of the ε-Cu phase contains approximately 7 wt % Co, while the circumference contains about 3.5 wt % Co. The ε-Cu dendrites were surrounded by yet a different phase, revealed by heavy etching, which according to X-ray microanalysis contains about 2–3 wt % Co as seen in Fig. 4a. The microstructure of samples which were quenched from a superheated melt had generally similar structures, but with a finer microstructural scale due to higher cooling rates. If the melt was supercooled below a certain temperature, depending on the original melt composition, liquid-phase separation was detected, generally in the form of dispersed Co-rich, sometimes distorted spheres (L1) embedded in a Cu-rich matrix (L2), as seen in Fig. 4b. Fig. 4b shows a Cu 15 wt % Co alloy supercooled to about 200 K below the liquidus and quenched on a Cu plate. The dark pear-shaped particle on the left side of the figure is the solidified L1 phase which contains about 80 wt % Co. The rest of the figure shows regions originating from solidification of the L2 phase, with an average composition of 10 wt % Co. Its microstructural characteristics are very similar to those of alloys solidified without supercooling, but with refined dimensions.

In Fig. 5 secondary electron images demonstrating the microstructure of Cu–15 wt % Co alloys solidified in the drop-tube are shown. The final form after solidification was that of flakes, 1 to 2 mm long, and about 30 to 50 μm thick. Fig. 5a and b present an SEM photograph of the same flake at two different magnifications. In the upper part one sees columnar cells, followed by a mixture of tiny spheres embedded in the matrix. In Fig. 5c the typical microstructure of the lower part of the flake is shown at a higher magnification. The microstructure consists of small spheres whose Co concentrations are higher than the average, embedded in a Cu-rich phase; the exact composition of a sphere could not be measured due to its small dimensions. A similar microstructure was observed in electron-beam surface-melted samples, which undergo solidification in the miscibility gap [11]. This point will be discussed later in detail.

SEM micrographs illustrating the characteristic microstructures of Cu–30 wt % Co solidified via EM levitation, as well as drop-tube experiments, are

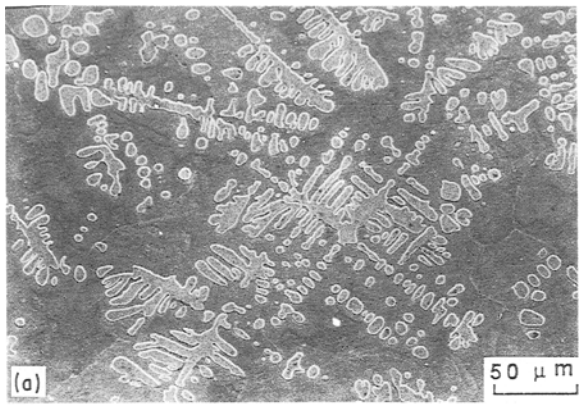

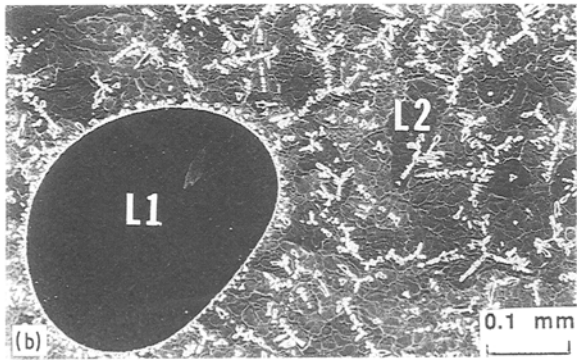

Figure 4 A series of secondary electron images illustrating the microstructure of Cu–15 wt % Co solidified via electromagnetic levitation: (a) sample dropped from the "solid + liquid" region; (b, c) sample solidified under 200 K supercooling.

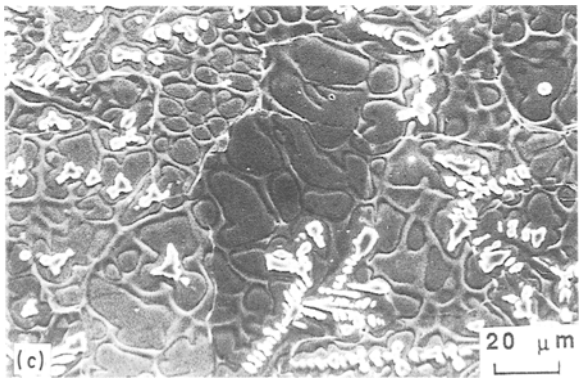

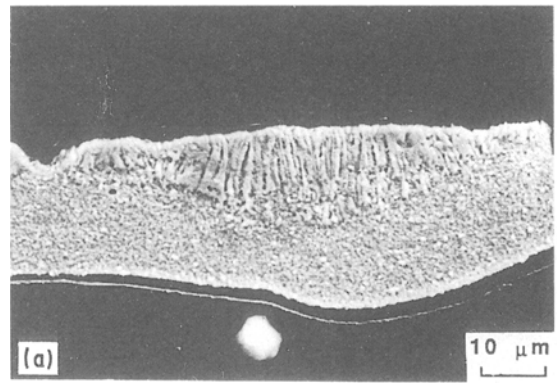

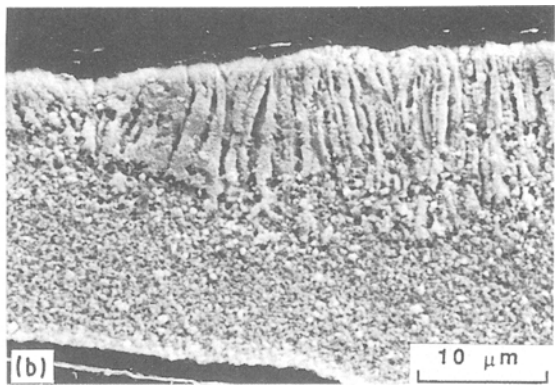

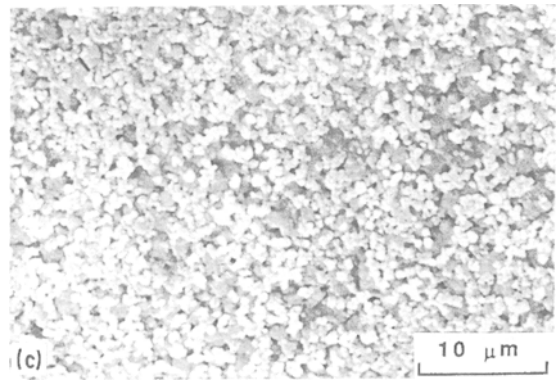

Figure 5 A series of secondary electron images demonstrating the microstructure of Cu–15 wt % Co flakes solidified in the drop-tube: (a, b) columnar growth followed by solidification in the miscibility gap; (c) a flake solidified in the miscibility gap.

shown in Fig. 6 and in Figs 7 and 8, respectively. Fig. 6 illustrates the microstructure of Cu–30 wt % Co which was supercooled by about 270 K prior to nucleation, i.e. the nucleation temperature T_n, is about 10 K below the peritectic temperature T_p [15]. In this sample, the L1 and L2 phases were found to contain 80 and 10 wt % Co, respectively. The microstructure exhibited features similar to those of the Cu–15 wt % Co alloys (compare Figs 4 and 6). In Fig. 7 the typical microstructure of Cu–30 wt % Co solidified in a drop-tube is shown. The dark rounded phase in the figure is the L1 phase, which is embedded in an L2 matrix. The Co concentration in the L1 and L2 phases was 82 and 9 wt %, respectively. According to our previous work [10], such Co concentrations indicate that an effective bulk supercooling as high as 300 K was achieved, i.e. $T_n \simeq T_p - 30$ K. The upper (flat) side of the sample shown in Fig. 7a can be assumed to be the one which was splattered against the drop-tube floor. As will be discussed later, at the moment of contact with the floor this specimen was in the "liquid + solid" region of the phase diagram (i.e. just after recalescence). As a result of the impact, it splits into many fragments. Each fragment recoils, and falls again on the drop-tube floor, where it finally solidifies in the form of a flake. In many cases, as illustrated in Fig. 7a, the fragment was still in the "liquid + solid" region when it touched the floor for the second time. The side touching the floor undergoes relatively high cooling rates. The microstructure is therefore very fine (Fig. 7d). The other side (lower fragment side in Fig. 7a), which solidified via much lower cooling rates, exhibits a coarser microstructure (Fig. 7c). For several flakes, small (sub-micrometre) spheres containing Co concentrations higher than the average were revealed, which is typical of specimens solidifying in the miscibility gap via high cooling rates [10].

There are two main differences between microstructural features seen in the EM levitation processed, and drop-tube processed specimens: (a) in the drop-tube samples, the L1 phase is more agglomerated, and does not have sub-features under the present resolution; and (b) dendrites or dendrite fragments are not observed in the L2 phase regions. Also, in one of the flakes a unique microstructure could be observed,

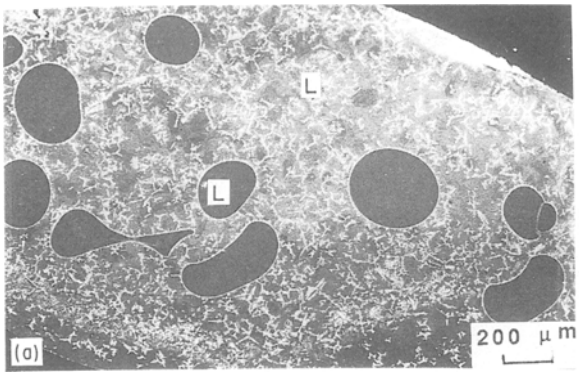

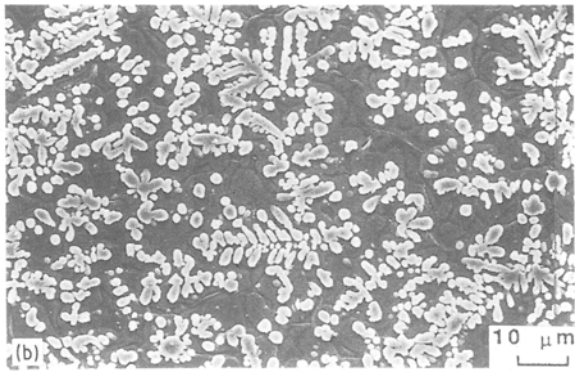

Figure 6 A series of secondary electron images showing the microstructure of Cu–30 wt % Co solidified via electromagnetic levitation: (a) overall view, (b) higher magnification of L2 liquid phase.

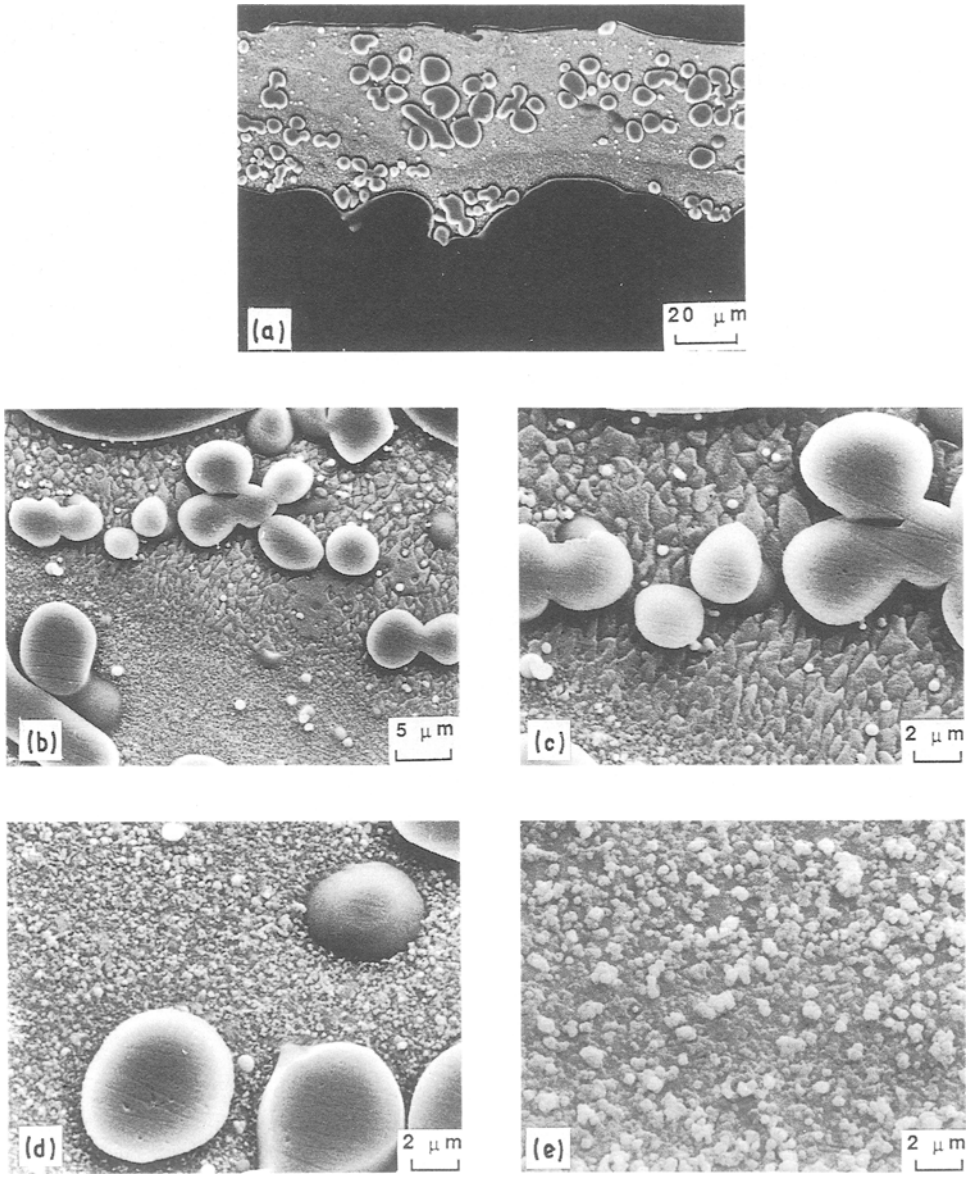

Figure 7 A series of secondary electron images illustrating the microstructure of Cu–30 wt % Co flakes solidified in the drop-tube: (a–d) different magnifications of the same flake. The splat edge (top side of (a)) has fine structure (d) while the other side with lower cooling rates has a coarser structure (c). (e) A different flake solidified under high cooling rates.

as illustrated in Fig. 8: the brighter phase is Co-rich dendrites embedded in a Cu-rich phase. In this flake, the typical L1 spheres could not be seen. Instead, fan-like dendrites as in Fig. 8b could be observed. We suggest that these dendrites are a result of diffused L1 phase due to an enhanced supercooling.

In Figs 9 and 10 we present SEM micrographs illustrating the microstructure of Cu–50 wt % Co solidified in the drop-tube from the "liquid + solid" and from the supercooled state, respectively. The final form of samples which were dropped after nucleation had already started was also in the form of flakes. In these samples, the first to solidify were Co dendrites, as can be seen in Fig. 9. The Co dendrites contained about 81.5 wt % Co embedded in a Cu-rich matrix, the latter containing only 10 wt % Co. The microstructure of specimens dropped in the liquid state underwent supercooling during the fall, and exhibited a complex structure as in Fig. 10. The big dark dendrites in Fig. 10a are primary Co dendrites containing about 81 wt % Co. The presence of small spheres, which contained between 76 and 80 wt % Co, indicates that the drop was supercooled to about 250–300 K and separated into two liquids. The L1 phase has a spherulitic shape while the L2 has either a grained structure, like that of Fig. 10a, or appears as very tiny precipitates, as in Fig. 10d.

4. Discussion

Assuming that the major heat dissipation of a falling drop is radiative, the solidification time t_s required to completely solidify the molten drop in an evacuated drop-tube after the onset of solidification is given by [21]:

$$t_s = \frac{mH_F}{\varepsilon A\sigma T_m^4 T_o^4} \quad (1)$$

where m is the dropped mass, H_F the latent heat of fusion, ε the material emissivity, A the falling drop

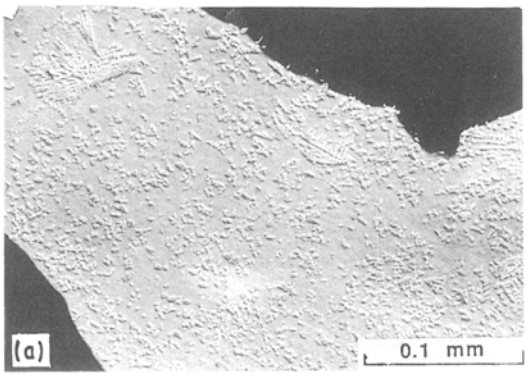

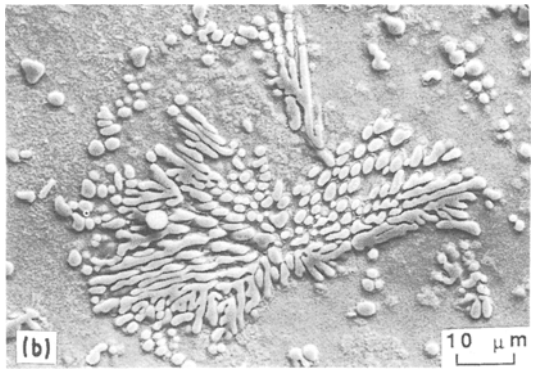

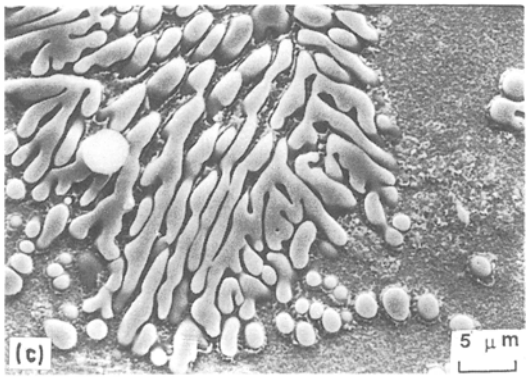

Figure 8 (a–c) A series of secondary electron images at different magnifications showing a discarded microstructure of Cu–30 wt % Co flakes solidified in the drop-tube.

surface area, σ the Stefan–Boltzmann constant, T_m the melting temperature and T_o the ambient temperature. Insertion of the values for the Cu–Co alloys in Table I into Equation 1 yields a total solidification time of about 20 s. This time is considerably longer than the 4.61 s available in the drop-tube. Therefore, the specimen which was dropped just after the nucleation onset will still be in the "liquid + solid" region of the phase diagram at the moment of splat.

Upon impinging on to the floor it splits into many fragments. Each fragment recoils, and falls again on the floor where it finally solidifies in the form of a flake. In this case a coarse dendritic structure is obtained. Dendrites as long as 300 μm could be observed with an average secondary dendrite arm spacing of about 6 μm (Fig. 9a), as expected at these solidification rates [10].

If the drop does not begin to solidify after release, it will lose heat and the molten drop might get supercooled. Following Wills and Katz [22], we assume that the material parameters of the supercooled liquid do not change during the free-fall duration, that the drop is spherical, that it is sufficiently small (so that there is only negligible thermal lag between the surface and centre), and that the drop tube is evacuated (i.e. radiative cooling only). Then, the cooling time t and the temperature reached T are related by [22]

$$t = \left\{4K_o T_o^3\left[\ln\left(\frac{T + T_o}{T - T_o}\right) + 2\tan^{-1}\left(\frac{T}{T_o}\right) + \ln\left(\frac{T_i + T_o}{T_i - T_o}\right) + 2\tan^{-1}\left(\frac{T_i}{T_o}\right)\right]\right\}^{-1} \quad (2)$$

where $K_o = \varepsilon A\sigma/mC_p$, C_p being the specific heat, T_i is the initial temperature, T_o is the ambient temperature and T is the temperature reached at time t after release. Inserting the appropriate values from Table I and the recalescence time for the different specimens (Table II) into Equation 2 yields a supercooling larger than about 300 K. Only a fraction of the melt, f_s^o, solidifies due to recalescence, and may be calculated from the equation [23]

$$f_s^o = \frac{C_p}{H_F(T_m - T)} \quad (3)$$

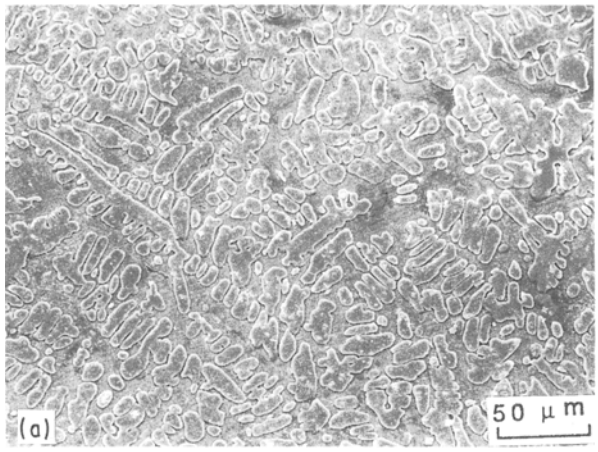

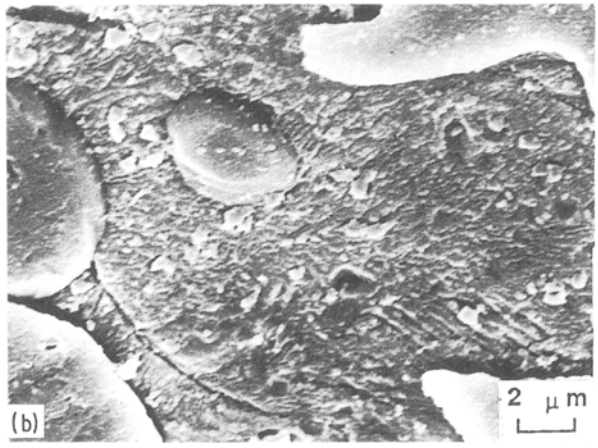

Figure 9 A series of secondary electron images demonstrating the microstructure of Cu–50 wt % Co flakes solidified in the drop-tube from the "solid + liquid".

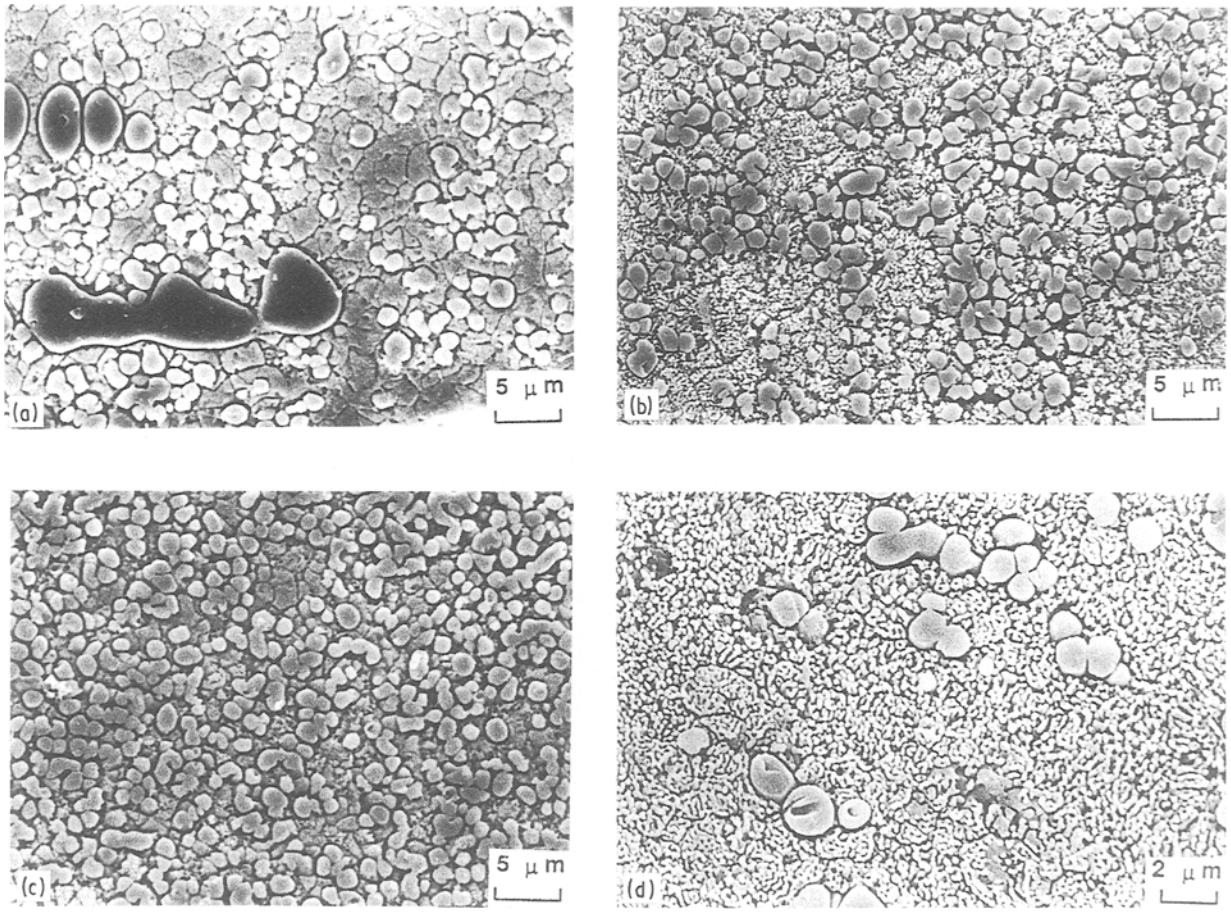

Figure 10 A series of secondary electron images demonstrating the microstructure of Cu–50 wt % Co flakes solidified in the drop-tube under about 300 K supercooling: (a–d) the different microstructures observed.

TABLE I Data for calculating the supercooling obtained during free fall

	Cu–15 wt % Co	Cu–30 wt % Co	Cu–50 wt % Co
Melting point (K)	1593	1663	1678
Heat capacity ($J g^{-1} K^{-1}$)	0.3967	0.4080	0.4209
Heat of fusion ($J g^{-1}$)	211.8	211.8	211.8
Emissivity	0.183	0.216	0.266
Drop radius, r (cm)	0.22	0.22	0.22
Stefan-Boltzmann constant ($J s^{-1} cm^{-2} K^{-4}$)	5.7×10^{-12}	5.7×10^{-12}	5.7×10^{-12}

TABLE II Calculations from data in Table I

Composition, Co (wt %)	Recalescence time (s)	Release temperature (K)	Supercooling (K)		Fraction of solid, f_s°
			Calc.[a]	Exp.	
15	4.52	1750	50	> 160	0.30
30	4.58	1775	90	300	0.58
50	4.40	1775	130	230	0.46

[a] Calculated according to the relative contribution of pure Cu and pure Co.

Since the specimen hits the drop-tube floor a very short time after recalescence, a residual melt, which did not have sufficient time to completely solidify, will still exist at the moment of splat. We suggest that just before this instant, a complete two-melt separation can occur as described by Gelles *et al.* [23]. These authors reported the formation of a massively separated Al-rich phase in Al–In alloys solidified under low-gravity conditions in space-shuttle flights. They explained the macroscopic Al-rich phase as a result of the coalescence of smaller Al-rich spherical droplets. For example, the coalescence was thought to proceed

by the collision of liquid droplets in the course of their migration to the warmer interior of the alloy during the cooling of a supercooled melt. Upon impact with the floor the drop splits into many fragments. At that very moment the completely separated liquid is forced to split into many fragments. However, an agglomeration tendency of the Co-rich phase (L1) may still be observed (Fig. 7a). Thus, the solidification behaviour in the drop-tube is completely different from the solidification characteristic of the EM levitation process samples [10]. In the drop-tube experiments, the fluid flow is minimized and diffusion acts as the driving force for merging, as stated above. In the levitation apparatus, large convection exist due to the electromagnetic stirring. In this case, two opposing forces are in operation: first, the merging of two small drops acting to reduce the surface energy (the kinetic energy excess finally dissipates as heat); second, if the kinetic energy of two colliding spherical L1 drops is larger than the energy needed to invest in surface-area enhancement the drops will tear into several smaller spherical drops. Thus, the abundance of fine L1 species in the microstructure is quite large.

As described above, the supercooled drop hits the tube floor a few tenths of a second after recalescence, when it splits into many droplets. Between the recalescence and the instant of hitting the solidification proceeds. The remaining melt is heated and large thermal gradients are effected by the released heat of fusion due to the lack of convection. Thus, each droplet could have different solid-to-liquid ratios (f_s^o, see Equation 3) and a different mean temperature. The small fragments falling again on the floor solidify in the form of flakes. Each flake solidifies along a different path dictated by the solid-to-liquid ratio at the second moment of contact, and on its mean temperature. The fraction solidified, f_s^o, could range between 0 and 1 and the temperature could range between the melting temperature T_m and the nucleation temperature T_n (up to about 300 K possible supercooling). This explains the variety of observed microstructures in a single experiment. As the flake touches the tube floor, high conductive heat dissipation starts. The typical thickness of the flakes ranged between 30 and 60 μm. Therefore, cooling rates as high as about 10^5 K s^{-1} [24] could be effected, yielding two unique microstructural features:

(i) *A sequence of columnar and two-melt separation microstructures.* If a droplet touches the tube floor when its temperature is higher than the separation temperature T_{sep}, it will grow initially in a columnar mode as seen in the top part of Fig. 6a. This type of microstructure is characteristic of rapid solidification of ribbons. However, the relatively high cooling rates imposed on the flake might cause supercooling in a part of the volume that is still liquid [11]. Supercooling below T_{sep} (which is also a function of composition) will cause melt separation, and a transition in the microstructure: the columnar structure transforms into a mixture of tiny spherulitic L1 particles embedded in a Cu-rich matrix, as seen in Fig. 5c. This structural type is characteristic of alloy solidification in the miscibility gap under high cooling rates [11].

(ii) *Discarded sphere microstructure.* This particular microstructure will be accounted for by assuming the existence of a lower temperature limit to the two-melt range in the metastable phase diagram, as proposed by Nakagawa [19] for the Cu–Co system. Below that particular temperature T_{misc} the system is again in a miscible metastable state. We consider an event of a droplet touching the tube floor while its temperature is lower than T_{sep}. The initial process which follows the floor contact is an additional supercooling [11] of most of the volume. The temperature might then decrease below T_{misc}. At that stage the two melts are under miscible conditions, and start to mix. However, the rapid cooling rates, i.e. short local solidification time, and lack of convection, inhibit complete mixing. The excess of Co in the L1 spheres diffuses radially, creating Co-rich liquid spherical zones, which then solidify in a regular dendritic manner as seen in Fig. 8b.

4.1. Evaluation of the degree of supercooling

Compositional analysis of L1 and L2 phases allows the estimation of the degree of supercooling by using the metastable phase diagram [19]. The supercooling obtained for several different experiments is given in Table II. These values agree with those calculated by Equation 2 if the emissivity constant of the alloys is taken as 0.6.

5. Summary

The microstructure of Cu–Co alloys solidified during a free fall (containerless solidification) was investigated. The following results were obtained.

1. Free fall of a spherical drop of Cu–Co alloy of about 3 mm in diameter may create a maximal supercooling of about $0.2T_m$. The constitutional details of the microstructure are consistent with the supercooling calculated on the basis of radiative heat loss in the evacuated tube.

2. The falling drops were in the "solid + liquid" state at the moment of impact on the drop-tube floor. Thus, a drop splits into many fragments which finally solidify as flakes upon touching the floor for the second time.

3. The microstructure of each flake depends on the degree of supercooling prior to solidification, which in turn depends on the solid fraction of the flake, its temperature, and on the flake thickness.

4. We suggest that just before the moment of impact, a complete melt separation occurred. Upon bumping on the tube floor, the complete separated melt L1 is forced to split into small L1 droplets.

5. We suggest that upon cooling below the separation temperature T_{sep} a Cu–Co liquid will separate into two liquids, one Co-rich (L1) and one Cu-rich (L2). However, cooling below T_{misc} will cause mixing of the two melts into one liquid. If sufficient time is

allowed for mixing a homogenized liquid is obtained, otherwise a discarded spherical structure is obtained.

Acknowledgements

The support of this research by the Office of Naval Research is gratefully acknowledged. The Scientific Officer of the programme was Dr Bruce A. MacDonald. Special thanks are due to Mr C. Cotler and Mr Z. Barkai for their assistance in the sample preparations.

References

1. A. MUNITZ and G. J. ABBASCHIAN, in Proceedings, "Undercooled Alloy Phases", New Orleans, Louisiana, March 1986, edited by C. C. Koch and E. W. Collings (Metallurgical Society of AIME) pp. 23–48.
2. D. D. McDEVITT and G. J. ABBASCHIAN, in Proceedings, "Chemistry and Physics of Rapidly Solidified Materials", St. Louis, Missouri, October 1982, edited by B. J. Berkowitz and R. O. Scattergood (Metallurgical Society of AIME) p. 49.
3. W. J. BOETTINGER, S. R. CORIEL and R. F. SEKERKA, in Proceedings, "Rapid Solidification Processing and Technologies", Gaithersburg, Maryland, December 1982, edited by R. Mehrabian, p. 45.
4. G. J. ABBASCHIAN and M. C. FLEMINGS, *Met. Trans. A* **14A** (1983) 1147.
5. T. Z. KATTAMIS and M. C. FLEMINGS, *Trans. TMS-AIME* **236** (1966) 1523.
6. *Idem., Trans. AFS* **75** (1967) 191.
7. T. F. KELLY and J. B. VANDER SANDE, in Proceedings, "Chemistry and Physics of Rapidly Solidified Materials", St. Louis, Missouri, October 1982, edited by B. J. Berkowitz and R. O. Scattergood (Metallurgical Society of AIME) p. 35.
8. L. M. HOGAN, in "Physics of Materials", edited by D. W. Borland, L. M. Clarebrough, and A. J. M. Moore (University of Melbourne, Australia, 1979) p. 111.
9. J. A. PATCHETT and G. J. ABBASCHIAN, *Met. Trans. B* **16B** (1985) 505.
10. A. MUNITZ, S. ELDER and G. J. ABBASCHIAN, Unpublished work (1991).
11. A. MUNITZ, *Met. Trans. B* **18B** (1987) 565.
12. R. E. CECH and D. TURNBULL, *Trans. AIME* **206** (1956) 124.
13. E. MEYER and L. RINDERER, *J. Crystal Growth* **28** (1975) 197.
14. L. S. NELSON, *Nature* **207** (1965) 741.
15. T. NISHIZAWA and K. ISHIDA, *Bull. Alloy Phase Diag.* **5** (1984) 161.
16. R. N. DOKKEN and J. F. ELLIOTT, *Trans. Metall. Soc. AIME* **233** (1965) 1351.
17. L. TIMBERG, J. M. TOGURI and T. AZAKAMI, *Met. Trans. B* **12B** (1981) 275.
18. P. TASKINEN, *Z. Metallkde* **73** (1982) 445.
19. Y. NAKAGAWA, *Acta Metall.* **6** (1958) 704.
20. S. J. B. REED, "Electron Microprobe Analysis" (Cambridge University Press, Cambridge, 1977) pp. 175–197.
21. M. B. ROBINSON, "Radiative and gas cooling of falling molten drops", NASA TM-78189 (Marshall Space Flight Center, Alabama, 1978).
22. F. D. WILLS and L. KATZ, "Solution to the differential equation for combined radiative and convective cooling for heated sphere", NASA TM X-73323 (Marshall Space Flight Center, Alabama, 1976).
23. S. H. GELLES, A. J. MARKWORTH and C. E. MOBLEY, in Proceedings of 4th European Symposium on Materials Science under Microgravity, Madrid, Spain, April 1983, p. 307.
24. H. JONES, in "Treatise on Materials Science and Technology", Vol. 20, edited by H. Herman (Academic, New York, 1981) p. 1.

Received 14 September 1990
and accepted 7 March 1991